Variation in young ovine cortical bone properties in regions habitually exposed to tension versus compression

Sony Manandhar[a], Sara G. Moshage[a], Joshua Craggette[a], John D. Polk[c,d], Mariana E. Kersh[a,b,c,*]

[a] *Mechanical Science and Engineering, University of Illinois at Urbana-Champaign*
[b] *Beckman Institute for Advanced Science and Technology; University of Illinois at Urbana-Champaign*
[c] *Carle Illinois College of Medicine; University of Illinois at Urbana-Champaign*
[d] *Program in Human Biology; University at Albany*

Abstract

Significant effort continues to be made to understand whether differences exist in the structural, compositional, and mechanical properties of cortical bone subjected to tensile vs. compressive loading. We evaluated these properties in juvenile sheep femora (age = 4 months). Cortical samples were machined from the anterior (tensile) and posterior (compressive) quadrants and at three points along the diaphysis. MicroCT scans (50 micron) were used to measure cortical thickness and mineral density. Three point bending tests were performed to measure the flexural modulus, strength, and post-yield displacement up to maximum force. There was no difference in cortical thickness between the tensile and compressive quadrants in any diaphyseal region; however, density in the tensile quadrant was higher than the compressive quadrant in the proximal and middle diaphysis. Overall, density was highest in the mid-diaphysis. Modulus in the tensile quadrant of the proximal and distal diaphysis was higher than in compressive regions, and strength was consistently higher in tensile quadrants - with the highest strength occurring in the proximal and middle diaphysis. There were no significant differences in post-yield displacement - though the tensile quadrant tended to exhibit less ductility post-yield. Together, our results suggest that there is a differential response of bone to historical tensile vs compressive loading in terms of elastic bending modulus and mechanical strength. The origins of this difference may lie within the variation in mineral density we observed between the two regions. However, it is important to note that the juvenile bone of quadrupeds contains a mix of osteonal and plexiform bone. The role of the constituent components of bone still undergoing mineralization, in combination with the plexiform structure, remains to be explored. This data suggest that in young ovine cortical bone, modulation of strength occurs via increased mineralization in regions exposed to tension thereby providing a possible biomechanical target for exercise prescriptions.

Keywords: density, tension, compression, cortical, growth, mechanical properties

1. Introduction

Osteoporosis and osteopenia are skeletal conditions characterized by a systematic loss in bone quality and increase in bone fragility. One option for improving bone health is via exercise in which the adaptation to mechanical stimuli can be exploited to encourage bone formation [1, 2, 3]. The development of exercise interventions for bone health would benefit from a better understanding of how bone adapts to specific strain modes.

Mechanical loading incurred from movement is known to be critical for the development of robust weight-bearing bones. For example, strains

*Corresponding author
Email address: mkersh@illinois.edu (Mariana E. Kersh)

in the femoral neck during walking are maximum inferiorly and smaller superiorly [4]. Accordingly, the inferior cortex is thicker than the superior cortex [5] suggesting a correspondence between mechanical strain and bone development. Numerous in vivo studies in a range of mammalian species have investigated the magnitude and frequency of loading that results in bone adaptation under physiological and experimental conditions [2, 6, 7, 8, 9, 10, 11].

While the magnitude of mechanical loading has been shown to affect bone adaptation, the specific mode of loading (e.g. tensile or compressive) is also important to the process of bone growth. Some studies report increased porosity, mineral content, and new remodeling events in regions of bone exposed to compressive strains compared to tensile strains [12, 13, 14, 15]. However, others report higher remodeling, yield strain, ultimate strain and Young's modulus in tensile regions compared to compressive [13, 14, 16]. Still others found no difference in the mechanical, structural or compositional properties of cortical bone in regions subjected to tensile and compressive loads [17, 18]. Therefore, whether bone growth occurs differently in regions of tension or compression remains unclear.

One limitation of previous work is the lack of characterization of both structural and material properties. Further, in those studies that performed mechanical testing, either tensile or compressive testing was performed - but not both. Strain mode (tension vs. compression) is an important factor in the mechanical evaluation of bone because cortical bone fails by different mechanisms when loaded in tension versus compression [19]. Moreover, most studies chose a single cross-section of bone for analysis, thus, the degree of spatial heterogeneity in bone properties along the diaphysis - and it's sensitivity to mechanical loading - remains unclear.

Consequently, our aim was to provide a more comprehensive understanding of how cortical bone growth is affected by the local strain environment using sheep femur as a model system. Our aims were to (1) evaluate whether bone properties differ between regions that habitually experience tension vs. compression, and (2) evaluate if bone growth is heterogeneous along the diaphysis. The overarching goal was to elucidate differences in bone growth in response to local mechanical loading and thus inform the development of targeted exercise interventions designed to reduce fracture risk.

2. Materials and Methods

Femoral bone samples from juvenile sheep were used for all analyses. To summarize, intact samples were first micro-CT scanned to analyze cortical thickness and density along the diaphysis. All image processing was performed semi-automatically using custom MATLAB code (Mathworks). Next, three sub-regions along the diaphysis were defined from which parallelopiped samples were machined and mechanically tested in 3-point bending. Details of all analyses are described in the remaining sections.

2.1. Subjects

Five juvenile Hampshire sheep were housed in a large indoor pen at the University of Illinois Sheep and Beef Cattle facility. All sheep were able to move freely while in the pen and access to food and water was not limited. Subjects were humanely euthanized at the age of 120 days, limbs were dissected, muscles and ligaments were removed, and the remaining bone segments were frozen at -20°C. All protocols were approved by the Institutional Animal Care and Use Committee at University of Illinois at Urbana-Champaign (UIUC).

2.2. Bone Imaging and Image Processing

Intact sheep femora were thawed and micro-computed tomography (microCT) data were acquired (Inveon, Siemens) at an isotropic 50 μm voxel size (80 kVp, 20 cm field of view, 1472x1472 matrix size). Three hydroxyapatite phantoms (density = 25, 100, 500 mg/cm^3, Model 092, CIRS) were included in the scans to convert Hounsield Units to hydroxyapatite density.

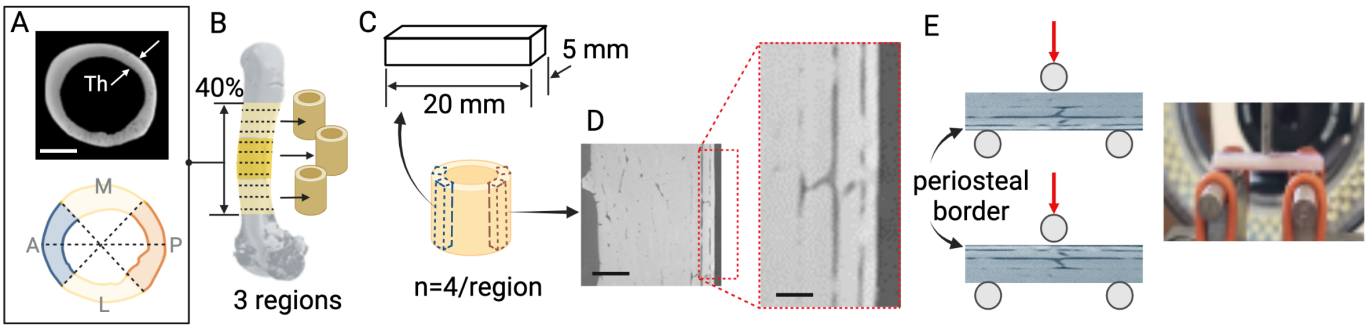

Figure 1: (A) MicroCT images at ten locations along the length of the diaphysis were used to quantify cortical thickness and density in the anterior and posterior quadrants (lower image). (B). For each femur, the diaphysis was separated into three regions: proximal, middle, and distal. (C) Two parallelopiped samples were machined from each quadrant and region of the diaphysis. (D) Transverse image of a sample scanned at 5 μm voxel size with evidence of circumferential bone along the periosteal border. (E) Test configurations used for each anatomical quadrant in which the periosteal border was either in compression or tension,

The diaphysis was defined as the middle 40% of total bone length and ten equally spaced transverse slices were then identified along the diaphysis (Fig. 1B). The diaphysis was sub-divided into three regions by thirds resulting in a proximal, middle, and distal diaphyseal regions per sample with corresponding transverse slices used to quantify thickness and density within each region.

Each CT image was individually binarized using a global threshold based on Otsu's method (Fig. 1A). Next, the centroid of the transverse slice was calculated and voxels along the periosteal border were identified. The border was discretized into 360 segments radiating outward from the centroid of the image with the origin of a polar coordinate system set at the centroid. The anterior and posterior anatomical quadrants were then identified (Fig. 1A, bottom).

2.3. Thickness and Density Measurements

Cortical thickness was calculated using the binarized images and defined as the distance between the periosteal and endosteal border within each anatomical quadrant of interest and in each longitudinal region of the diaphysis. For example, within the slices corresponding to proximal diaphysis (the proximal three slices), the median of all thickness measurements in the anterior quadrant was calculated. This process was repeated for the posterior quadrant of the proximal diaphysis, and similarly for the middle and distal regions of the diaphysis where the middle four slices were used for the mid-diaphysis and distal three slices used for the distal diaphysis.

The binarized images were used to segment the microCT data for measurement of mineral density within each quadrant and region along the diaphysis. Subject specific hydroxyapatite calibration curves were used to convert microCT Hounsfield units to tissue mineral density. The average density within the slices corresponding to the anatomical quadrant and region of interest was calculated.

2.4. Sample Preparation

The location of the central 40% of the femoral diaphysis was measured on each bone sample and marked. The regions proximal (femoral head and epiphysis) and distal (epiphysis and condyles) to the diaphysis were removed using a diamond band saw (Model C-40, Gryphon). Next, the diaphysis was potted within custom 3D-printed fixtures using Bondo and then secured within the bed of a 5 Axis CNC machine (Model HY6040, Chinazone). Two parallelopiped full-thickness samples (20mm x 5mm x cortical thickness) were milled from each anatomical quadrant (Fig. 1C) using titanium coated 1-mm end mills (12000 RPM, 50% feed rate).

2.5. Mechanical Testing

All samples were tested in three-point bending. In a small imaging pilot study, a subset of the parallelopiped samples were scanned at 5 μm voxel size (10 W and 50 kV, Model MicroXCT-400, Zeiss Xradia). We observed a consistent ring of circumferential cortical bone on the periosteal surface of all samples (Fig. 1D). Two configurations of testing were therefore used to account for whether or not the circumferential bone would influence our mechanical test results: strain mode specific (SMS) and non-strain mode specific (xSMS).

The purpose of the SMS condition was to test samples in the expected physiological loading condition. For the anterior quadrant, this corresponds to the periosteal side in tension while samples from the posterior quadrant would have the periosteal side in compression (Fig. 1E). The non-strain mode specific condition is the reverse: the periosteal side would be in compression for anterior samples and tension for posterior samples. Detailed diagrams of the test setup can be found in the supplementary materials.

Each bone sample was submerged in PBS for at least 15 minutes prior to testing to ensure it was hydrated. The sample was placed on support pins (diameter = 4 mm) of a three-point-bend test fixture (span = 15 mm) for use in a mechanical test machine (MTS criterion 43, Instron). Each sample was loaded to failure at a rate of 0.01 mm/sec in displacement control and force and was measured with a 1kN load cell. Displacement was measured using the cross-head displacement of the test machine. The test was ended if either the sample failed or when the displacement limit of 2 mm was reached.

Post-processing of mechanical test data was performed in Matlab (Mathworks R2019b). The linear region of the load-displacement curve was identified using an iterative correlation in which the start and end points (up to maximum force) were selected such that the strength of the linear regression between these points was maximized (threshold: r=0.999). For each sample, the bending modulus (E_B) and strength (S_B) was calculated using linear elastic beam theory:

$$E_B = \frac{m * L_s^3}{4 * w * Th^3} \quad (1)$$

$$S_B = \frac{3 * F * L_s}{2 * w * Th^2} \quad (2)$$

where m is the slope from the linear region of the load-displacement curve, F is the maximum load during mechanical testing, L_s refers to the span length (15 mm), and w and Th are the width (5 mm) and the thickness of the specimen, respectively. Post-yield displacement was defined as the displacement occurring between yield (end of linear region) and maximum force.

2.6. Statistical Analysis

Normality of data was tested using a Shapiro-Wilk test with a significance level of 0.05. Since some data were not normally distributed, summary data is presented as medians and median absolute deviations. Inter-group comparisons were performed using a paired samples Wilcoxon Test (significance level = 0.05) accounting for samples from the same bone and locations within each quadrant. All analyses were performed in RStudio (Version 1.2.5033).

3. Results

3.1. Cortical thickness and density

We successfully machined pairs of parallelopipeds from the anterior and posterior quadrants along the three regions of the diaphysis (n=12 total/bone). Of the parallelopipeds machined from the same anatomical quadrant , there was no difference in either cortical thickness or density between the pairs (Table S1). We therefore pooled the samples within each anatomical quadrant to evaluate cortical thickness and density between quadrants and in regions along the diaphysis.

We found no significant differences in anterior cortical thickness versus posterior cortical thickness (p-range= 0.11-0.69, Table 1) within any given region of the diaphysis. Cortical thickness within the anterior diaphysis was 2.39 $\pm$ 0.41 mm and 2.48 $\pm$ 0.26 mm in the posterior diaphysis

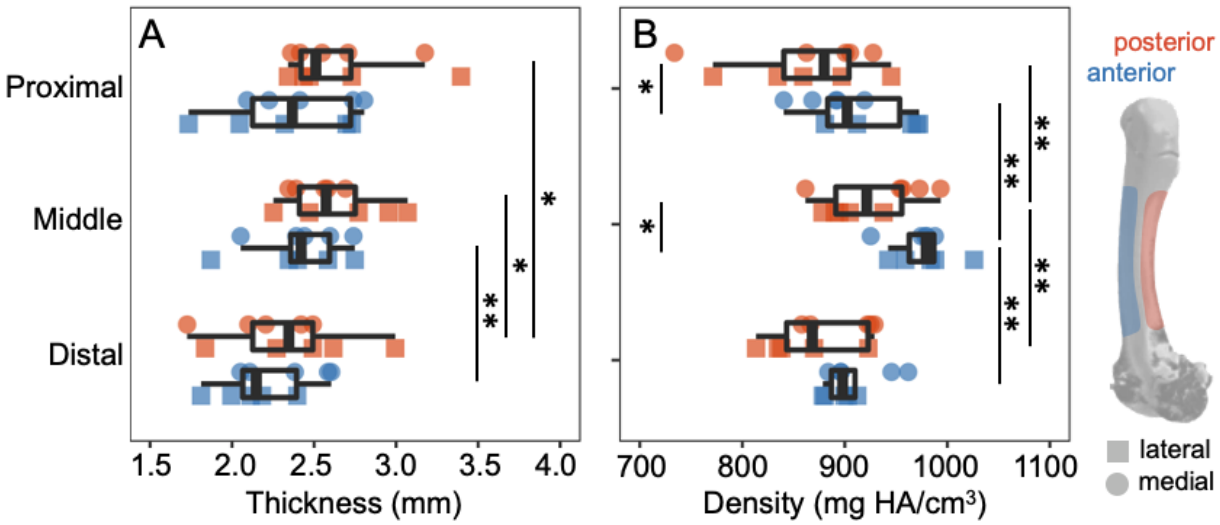

Figure 2: Cortical thickness (A) and density (B) in the anterior(blue) and posterior (orange) anatomical quadrants along different regions of the diaphysis. Circles and squares indicate samples taken nearer to the medial or lateral aspect, respectively. Cortical thickness was uniform while density in the anterior quadrant was highest in the mid-diaphysis. $*p < 0.05, **p < 0.01$

(Fig. 2A). Cortical thickness in the distal diaphysis was significantly thinner than the mid-diaphysis for both anterior (-11%, p=0.0019) and posterior quadrants (-8.6%, p=0.019).

In contrast to thickness, density in the anterior quadrant was higher than the posterior quadrant in the proximal (2.5%, p=0.049) and middle diaphysis (6.3%, p=0.037, Fig. 2B). Mineral density was consistently higher in the mid-diaphysis compared to the proximal and distal diaphysis (p-range = 0.0019-0.0098, Table 1). However, the increase in mid-diaphyseal density was greater in the anterior quadrant (8.8%) compared to the posterior quadrant (5.4%).

3.2. Bending modulus, strength, and plastic deformation

The bending modulus within each anatomical quadrant was insensitive to whether the periosteal side was in compression or tension (SMS vs xSMS, Table S2). Overall, the bending modulus in the anterior quadrants were higher than the posterior quadrants (Figure 3D, Table 2) with significant increases in the proximal (47%, p=0.0039) and distal diaphysis (22%, p = 0.049). Within a given quadrant, there were no significant differences along the diaphysis.

Differences in bending strength of the anterior and posterior quadrant were more pronounced (Figure 3E). Strength in the anterior quadrant of was 62% higher (p=0.0019) than the posterior quadrant in the mid-diaphysis, 50% higher in the proximal diaphysis (p=0.0019), and 21% higher in the distal diaphysis (p=0.037). When comparing strength along the longitudinal axis of the diaphysis, the largest differences were in the anterior quadrant with strength in the proximal and middle regions on average 22% higher than the distal region (p-range = 0.014-0.048). Within the posterior quadrant, there was a 9.7% increase in proximal strength compared to the mid-diaphysis (p=0.037).

Finally, the amount of post-yield displacement were greater in the posterior than anterior quadrant though there were no statistically significant differences (p=range = 0.064 - 0.49). Within the anterior quadrant, the post-yield displacement in the middle diaphysis was 64% higher than the distal diaphysis (Figure 3F). There were no significant differences along the diaphysis within the posterior quadrant.

Region	Quadrant	Thickness (mm)				
		Median (MAD)	Regions (p-value)	Quadrant (p-value)		
Proximal (P)	Anterior	2.37 (0.48)	0.14		P v M	0.69
	Posterior	2.51 (0.24)		Ant	P v D	0.23
Middle (M)	Anterior	2.42 (0.25)	0.11		M v D	**0.0019**
	Posterior	2.57 (0.28)			P v M	0.69
Distal (D)	Anterior	2.15 (0.29)	0.69	Post	P v D	**0.027**
	Posterior	2.35 (0.29)			M v D	**0.019**
Region	Quadrant	Density (mg HA/cm^3)				
		Median (MAD)	Regions (p-value)	Quadrant (p-value)		
Proximal (P)	Anterior	902.37 (41.20)	**0.049**		P v M	**0.0059**
	Posterior	879.89 (52.50)		Ant	P v D	0.77
Middle (M)	Anterior	979.32 (12.98)	**0.037**		M v D	**0.0019**
	Posterior	921.45 (49.76)			P v M	**0.0098**
Distal (D)	Anterior	897.92 (21.07)	0.69	Post	P v D	0.56
	Posterior	868.30 (64.75)			M v D	**0.0059**

Table 1: Cortical thickness and density in each region along the diaphysis. Within each region, thickness and density was compared between anterior and posterior quadrants (n=10/quadrant). Differences along the diaphyseal regions, within the same quadrant (e.g. proximal anterior vs middle anterior) were also compared. Density in the middle anterior diaphysis was higher than the proximal and distal diaphysis. MAD = median absolute deviation.

4. Discussion

In this study we have used high-resolution imaging and mechanical test data to evaluate the degree of spatial heterogeneity in young cortical bone subjected to tension (anterior quadrant) vs. compression (posterior). Our data showed no difference in cortical thickness in regions of the diaphysis that habitually experience tension vs. compression, suggesting relatively uniform bone growth around the femoral diaphysis during early growth in sheep. However, thicker cortex has been reported in regions of compression (compared to tension) in the deer calcaneus [19] and rat tibia [20], while others have shown thicker cortex in the tensile regions of sheep radii [21] and equine metacarpus [13]. One explanation for the difference may be due to age. The studies summarized here were performed in skeletally mature bone, in contrast to our analysis of bone in early stages of post-natal development. It may be that during ontegeny, adaptations to increasing mass or speed (or a combination thereof) lead to regional variations. Our data suggests that in early growth, sheep femora begin with uniform cortical thickness at the cross-sectional level - though we did observe differences along the diaphysis with the distal diaphysis having the thinnest cortex.

In contrast to thickness, our comparison of mineral density revealed increased mineralization levels in bone under tension versus compression with the greatest difference occurring in the mid-diaphysis. Again, our data is in contrast to mineral content reported in deer calcaneus [19] and human tibia [22] but in agreement with data from the equine metacarpus [13]. When compared longitudinally, the anterior mid-diaphysis was at least 8% more mineralized than the proximal or distal diaphysis, and similar but lower differences (5.4% more mineralized) were found in the posterior quadrant.

During movement, long bone deformation causes pressure gradients to drive fluid flow within bone and has been hypothesized to flow from regions of compression to regions of tension [23].

Region	Quadrant	Modulus (GPa)				
		Median (MAD)	Quadrant (p-value)	Regions (p-value)		
Proximal (P)	Anterior	4.89 (0.63)	**0.0039**	Anterior	P v M	0.16
	Posterior	3.33 (0.85)			P v D	0.084
Middle (M)	Anterior	3.94 (1.11)	0.065		M v D	0.38
	Posterior	2.79 (0.76)		Posterior	P v M	0.43
Distal (D)	Anterior	3.60 (0.87)	**0.049**		P v D	0.49
	Posterior	2.95 (0.52)			M v D	0.38
Region	Quadrant	Strength (MPa)				
		Median (MAD)	Quadrant (p-value)	Regions (p-value)		
Proximal (P)	Anterior	153.73 (17.81)	**0.0019**	Anterior	P v M	0.77
	Posterior	102.67 (4.77)			P v D	**0.048**
Middle (M)	Anterior	151.32 (12.55)	**0.0019**		M v D	**0.014**
	Posterior	93.61 (8.37)		Posterior	P v M	**0.037**
Distal (D)	Anterior	124.85 (16.28)	**0.037**		P v D	0.93
	Posterior	103.05 (15.21)			M v D	0.084
Region	Quadrant	Post-yield Displacement (mm)				
		Median (MAD)	Quadrant (p-value)	Regions (p-value)		
Proximal (P)	Anterior	0.21 (0.08)	0.32	Anterior	P v M	0.13
	Posterior	0.35 (0.29)			P v D	0.32
Middle (M)	Anterior	0.14 (1.5E-4)	0.064		M v D	**0.019**
	Posterior	0.27 (0.19)		Posterior	P v M	0.49
Distal (D)	Anterior	0.23 (0.11)	0.49		P v D	0.99
	Posterior	0.30 (0.11)			M v D	0.32

Table 2: Comparisons of mechanical test results: modulus, strength, and post-yield displacement between quadrants and along different regions of the diaphysis. MAD = median absolute deviation.

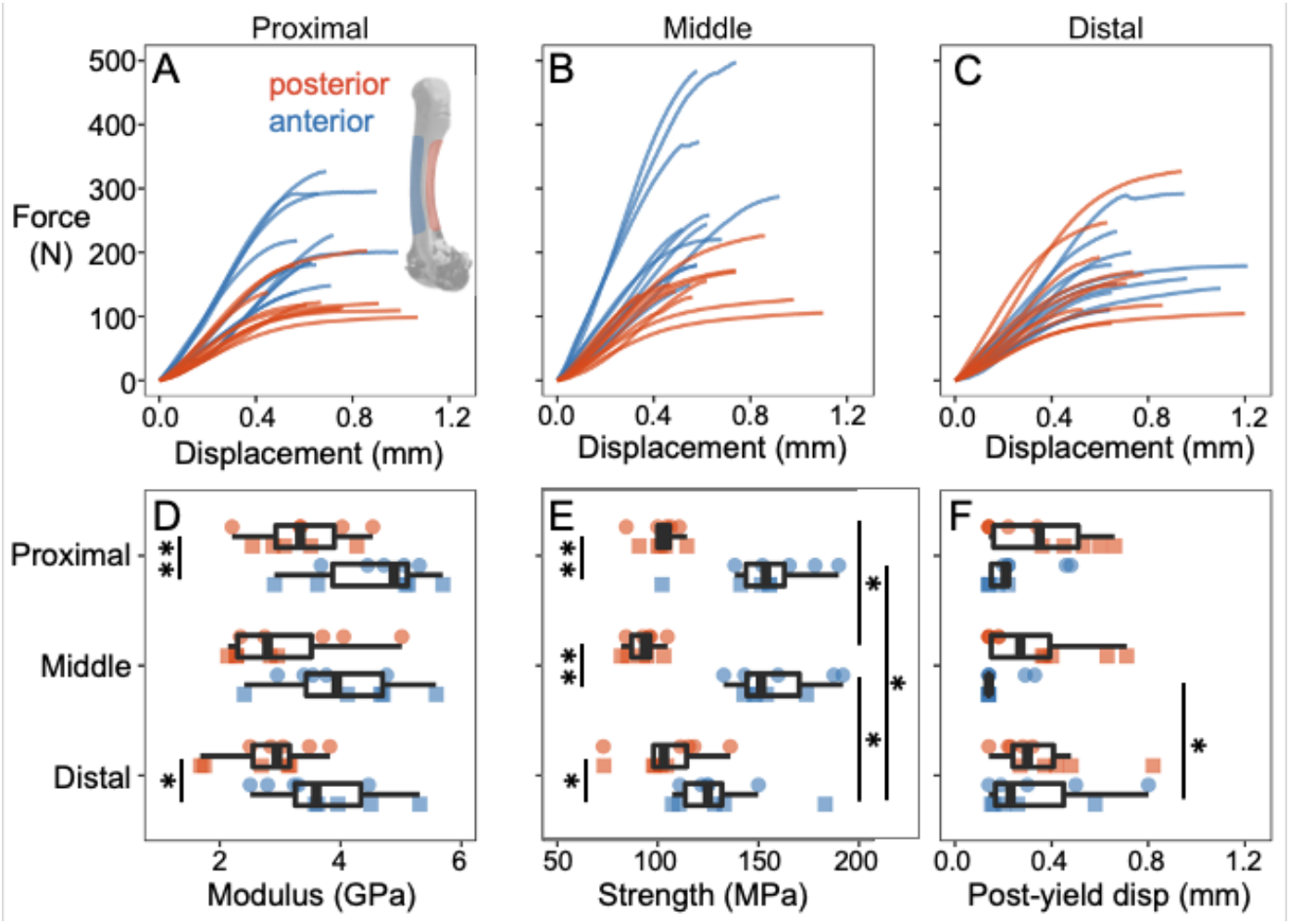

Figure 3: Cortical thickness (A) and density (B) in the anterior(blue) and posterior (orange) anatomical quadrants along different regions of the diaphysis. Circles and squares indicate samples taken nearer to the medial or lateral aspect, respectively. Cortical thickness was uniform while density in the anterior quadrant was highest in the mid-diaphysis. $*p < 0.05, **p < 0.01$

The resulting strains sensed by the osteocytes tethered to the bone matrix are 1-2 orders of magnitude greater than the tissue level strains generated by muscles [23, 24, 25, 26]. Long bones like the femur, tibia, and ulna are an ideal target for understanding the sensitivity of bone adaptation to loading mode because the inherent curvature leads to tensile strains on the convex side and compressive strains on the concave side [27].

Whether osteocytes in tensile regions are more activated than in compressive regions continues to be debated: Skedros and colleagues [28] reported significantly more remodeling events in the tensile cortex compared to the compressive cortex while the use of the tibia loading model in mice has shown decreased levels of sclerostin and correspondingly increased bone area in tensile regions [29]. While the underlying mechanism is unclear - our data indicate that for young ovine bone, mineral density was higher in tensile regions and was greatest overall in the mid-diaphysis where bending loads would be at a maximum.

We next turned to investigating how these changes in thickness and density manifested in differences in mechanical properties - a novel component of our study. We found that the elastic bending modulus was higher in regions of tension versus compression. Moreover, these differences were amplified with respect to strength where bending strength was up to 62% higher in the tensile quad-

rant and is likely attributable to the increase in mineralization. To our knowledge, there are only two studies that have tested cortical bone samples from both tension and compression regions of a bone [16, 17]). While Skedros et al. reported higher flexural modulus, yield and ultimate strain in samples from tensile regions of bone, Cuppone et al. reported no difference between the tensile and compressive quadrants.

Interestingly, while mineralization at the mid-diaphysis was greater than the proximal diaphysis - there was no difference in proximal or middle levels of strength in the tensile quadrants. Moreover, the compressive quadrant was moderately lower in strength at the mid-diaphysis. Thus, while the role of mineralization corresponded to differences in strength in tensile vs. compressive quadrants - the degree of spatial heterogeneity within a given quadrant along the length of the diaphysis was not fully explained by variation in mineralization levels. One reason may be related to the presence of plexiform bone which is known to occur in rapidly growing animals including sheep. In a study of goat femur, tensile regions were shown to have plexiform bone whereas compressive regions had more haversian bone [15].

Plexiform bone serves as an initial collagen-rich template for subsequent modeling and remodeling activity in which the plexiform bone is eventually replaced by haversion bone. Hence, the role of collagen in young bone may be another important determinant of strength. The collagen fibers in the equine third metacarpal cortex exposed to tensile loading were more longitudinal compared to the compressive lateral cortex [13]. Similarly, two separate studies on equine radius also demonstrated longitudinal collagen fiber orientation in the tensile cortex and oblique/transverse collagen in the compression cortex [30, 31]. While the relationship between collagen fiber orientation and bone strength seems to be undisputed, the mechanism of how it affects bone strength is not fully understood.

Our study has several noteworth contributions. To our knowledge, this work is the first to investigate structure, composition, and material properties of cortical bone in both physiological (SMS) and non-physiological loading (non-SMS) conditions. Our findings demonstrated that bone subjected to tensile loads is associated with increased strength regardless of testing mode (SMS vs. non-SMS). Moreover, we have demonstrated the degree of spatial heterogeneity along the diaphysis highlighting the potential for young growing bone to serve as a model for understanding natural modeling events in response to varying strain environments. Our data suggests that there is an increased response of bone to tensile strains via changes in mineralization and this may therefore serve as a biomechanical target for exercise studies aiming to improve bone properties.

However, our work is not without limitations. Our sample size is somewhat small and limited to a single time point of age. It remains to be demonstrated the degree to which these trends would be sustained during ontogeny. The lack of complete correspondence between mineralization levels and strength indicate a need to evaluate other metrics that may effect bone strength; namely structural variations in plexiform vs haversion bone and the role of collagen alignment.

In summary, we have shown the structural, compositional and material properties of cortical bone are affected differently in relation to the local mechanical environment. Furthermore, bone growth is spatially heterogeneous as seen from results along the longitudinal axis of the diaphysis and in comparing tensile vs compressive regions. Hence, this study will aid in developing a comprehensive understanding of young cortical bone growth in response to the local mechanical strain environment. Based on our experimental findings, cortical bone is stronger in regions subjected to habitual tensile loading than opposing regions subjected to compressive loading, and that this difference in strength is a consequence of mineral density. These results suggest that bone's modeling and remodeling processes can alter local bone strength and diminish fracture risk.

5. Conflict of Interest

None.

6. Acknowledgements

This study was funded by the National Science Foundation (NSF-1639756). Thank you to Hyunggwi Song for his assistance with developing portions of the image processing pipeline. We are grateful for the technical support from David Ehrhardt from Advanced Materials Testing and Evaluation Laboratory at UIUC and Dr. Leilei Yin and Travis Ross for their help with micro-CT scanning and post-processing technical support at the Beckman Institute, UIUC. Thanks also to Mark Pinson, Gary Sedberry and Kyle Cheek from the Mechanical Science and Engineering machine shop for their assistance. Portions of figures were generated using Biorender.

References

[1] A. Hammer, The paradox of Wolff's theories, Irish Journal of Medical Science 184 (1) (2015) 13–22. doi:10.1007/s11845-014-1070-y.

[2] A. G. Robling, K. M. Duijvelaar, J. V. Geevers, N. Ohashi, C. H. Turner, Modulation of appositional and longitudinal bone growth in the rat ulna by applied static and dynamic force, Bone 29 (2) (2001) 105–113. doi:10.1016/S8756-3282(01)00488-4.

[3] H. M. Frost, Bone "mass" and the "mechanostat": A proposal, The Anatomical Record 219 (1) (1987) 1–9. doi:10.1002/AR.1092190104.
URL https://onlinelibrary-wiley-com.proxy2.library.illinois.edu/doi/full/10.1002/ar.1092190104https://onlinelibrary-wiley-com.proxy2.library.illinois.edu/doi/abs/10.1002/ar.1092190104https://onlinelibrary-wiley-com.proxy2.library.illinois.edu/doi/10.1002/ar

[4] M. E. Kersh, S. Martelli, R. Zebaze, E. Seeman, M. G. Pandy, Mechanical Loading of the Femoral Neck in Human Locomotion, Journal of Bone and Mineral Research 33 (11) (2018) 1999–2006. doi:10.1002/jbmr.3529.
URL http://doi.wiley.com/10.1002/jbmr.3529

[5] M. E. Kersh, M. G. Pandy, Q. M. Bui, A. C. Jones, C. H. Arns, M. A. Knackstedt, E. Seeman, R. M. Zebaze, The heterogeneity in femoral neck structure and strength, Journal of Bone and Mineral Research 28 (5) (2013) 1022–1028. doi:10.1002/jbmr.1827.

[6] S. J. Warden, S. M. Mantila Roosa, M. E. Kersh, A. L. Hurd, G. S. Fleisig, M. G. Pandy, R. K. Fuchs, Physical activity when young provides lifelong benefits to cortical bone size and strength in men, Proceedings of the National Academy of Sciences of the United States of America 111 (14) (2014) 5337–5342. doi:10.1073/pnas.1321605111.

[7] C. H. Turner, D. B. Burr, Basic biomechanical measurements of bone: A tutorial, Bone 14 (4) (1993) 595–608. doi:10.1016/8756-3282(93)90081-K.

[8] A. G. Torrance, J. R. Mosley, R. F. Suswillo, L. E. Lanyon, Noninvasive loading of the rat ulna in vivo induces a strain-related modeling response uncomplicated by trauma or periostal pressure, Calcified Tissue International 54 (3) (1994) 241–247. doi:10.1007/BF00301686.

[9] A. M. Weatherholt, R. K. Fuchs, S. J. Warden, Cortical and trabecular bone adaptation to incremental load magnitudes using the mouse tibial axial compression loading model, Bone 52 (1) (2013) 372–379. doi:10.1016/j.bone.2012.10.026.
URL https://pubmed.ncbi.nlm.nih.gov/23111313/

[10] D. E. Lieberman, O. M. Pearson, J. D. Polk, B. Demes, A. W. Crompton, Optimization of bone growth and remodeling in response to loading in tapered mammalian limbs, Journal of Experimental Biology 206 (18) (2003) 3125–3138. doi:10.1242/jeb.00514.

[11] R. P. Main, Ontogenetic relationships between in vivo strain environment, bone histomorphometry and growth in the goat radius, Journal of Anatomy 210 (3) (2007) 272–293. doi:10.1111/j.1469-7580.2007.00696.x.

[12] L. E. Lanyon, D. G. Baggott, Mechanical function as an influence on the structure and form of bone, Journal of Bone and Joint Surgery - Series B 58 (4) (1976) 436–443. doi:10.1302/0301-620x.58b4.1018029.

[13] J. G. Skedros, M. W. Mason, M. C. Nelson, R. D. Bloebaum, Evidence of structural and material adaptation to specific strain features in cortical bone, Anatomical Record 246 (1) (1996) 47–63. doi:10.1002/(SICI)1097-0185(199609)246:1<47::AID-AR6>3.0.CO;2-C.

[14] J. G. Skedros, S. C. Su, R. D. Bloebaum, Biomechanical implications of mineral content and microstructural variations in cortical bone of horse, elk, and sheep calcanei, Anatomical Record 249 (3) (1997) 297–316. doi:10.1002/(SICI)1097-0185(199711)249:3<297::AID-AR1>3.0.CO;2-S.

[15] A. Mayya, A. Banerjee, R. Rajesh, Mammalian cortical bone in tension is non-haversian, Scientific Reports 3 (2013) 1–6. doi:10.1038/srep02533.

[16] J. G. Skedros, M. R. Dayton, C. L. Sybrowsky, R. D. Bloebaum, K. N. Bachus, The influence of collagen fiber orientation and other histocompositional characteristics on the mechanical properties of equine cortical bone, Journal of Experimental Biology 209 (15) (2006) 3025–3042. doi:10.1242/JEB.02304.

[17] M. Cuppone, B. B. Seedhom, E. Berry, A. E. Ostell, The Longitudinal Young's Modulus of Cortical

Bone in the Midshaft of Human Femur and its Correlation with CT Scanning Data, Calcified Tissue International 2003 74:3 74 (3) (2003) 302–309. doi:10.1007/S00223-002-2123-1.
URL https://link.springer.com/article/10.1007/s00223-002-2123-1

[18] I. J. Wallace, B. Demes, C. Mongle, O. M. Pearson, J. D. Polk, D. E. Lieberman, Exercise-induced bone formation is poorly linked to local strain magnitude in the sheep tibia, PLoS ONE 9 (6) (2014) 1–5. doi:10.1371/journal.pone.0099108.

[19] S. JG, B. RD, M. MW, B. DM, Analysis of a tension/compression skeletal system: possible strain-specific differences in the hierarchical organization of bone, The Anatomical record 239 (4) (1994) 396–404. doi:10.1002/AR.1092390406.
URL https://pubmed.ncbi.nlm.nih.gov/7978363/

[20] M. L. Knothe Tate, R. Steck, M. R. Forwood, P. Niederer, In vivo demonstration of load-induced fluid flow in the rat tibia and its potential implications for processes associated with functional adaptation, Journal of Experimental Biology 203 (18) (2000) 2737–2745.

[21] L. E. Lanyon, P. T. Magee, D. G. Baggott, The relationship of functional stress and strain to the processes of bone remodelling. An experimental study on the sheep radius, Journal of Biomechanics 12 (8) (1979) 593–600. doi:10.1016/0021-9290(79)90079-4.

[22] Y. M. Lai, L. Qin, V. W. Hung, K. M. Chan, Regional differences in cortical bone mineral density in the weight-bearing long bone shaft—A pQCT study, Bone 36 (3) (2005) 465–471. doi:10.1016/J.BONE.2004.11.005.

[23] Y. Han, S. C. Cowin, M. B. Schaffler, S. Weinbaum, Mechanotransduction and strain amplification in osteocyte cell processes, Proceedings of the National Academy of Sciences 101 (47) (2004) 16689–16694.

[24] A. G. Robling, L. F. Bonewald, The Osteocyte: New Insights, Annual Review of Physiology 82 (1) (2020) 485–506. doi:10.1146/annurev-physiol-021119-034332.

[25] R. Smalt, F. T. Mitchell, R. L. Howard, T. J. Chambers, Induction of NO and prostaglandin E2 in osteoblasts by wall-shear stress but not mechanical strain, American Journal of Physiology - Endocrinology and Metabolism 273 (4 36-4) (1997) 751–758. doi:10.1152/ajpendo.1997.273.4.e751.

[26] M. M. Thi, S. O. Suadicani, M. B. Schaffler, S. Weinbaum, D. C. Spray, Mechanosensory responses of osteocytes to physiological forces occur along processes and not cell body and require αvβ3 integrin, Proceedings of the National Academy of Sciences of the United States of America 110 (52) (2013) 21012–21017. doi:10.1073/pnas.1321210110.

[27] J. E. Bertram, A. A. Biewener, Bone curvature: sacrificing strength for load predictability?, Journal of theoretical biology 131 (1) (1988) 75–92.

[28] J. G. Skedros, M. W. Mason, R. D. Bloebaum, Modeling and remodeling in a developing artiodactyl calcaneus: A model for evaluating Frost's mechanostat hypothesis and its corollaries, Anatomical Record 263 (2) (2001) 167–185. doi:10.1002/ar.1094.

[29] A. Moustafa, T. Sugiyama, J. Prasad, G. Zaman, T. Gross, L. E. Lanyon, J. Price, Mechanical loading-related changes in osteocyte sclerostin expression in mice are more closely associated with the subsequent osteogenic response than the peak strains engendered, Osteoporosis International 23 (4) (2012) 1225–1234.

[30] C. M. Riggs, L. E. Lanyon, A. Boyde, Functional associations between collagen fibre orientation and locomotor strain direction in cortical bone of the equine radius, Anatomy and embryology 187 (3) (1993) 231–238. doi:10.1007/BF00195760.
URL https://pubmed.ncbi.nlm.nih.gov/8470823/

[31] M. W. Mason, J. G. Skedros, R. D. Bloebaum, Evidence of strain-mode-related cortical adaptation in the diaphysis of the horse radius, Bone 17 (3) (1995) 229–237. doi:10.1016/8756-3282(95)00213-W.

Supplemental Data

Region	Quadrant	Subsection	Thickness (mm)			Density (mg HA/cm3)		
			Median	MAD	p-value	Median	MAD	p-value
Proximal	Anterior	Lateral	2.32	0.56	0.31	964.95	11.24	0.063
		Medial	2.41	0.48		891.23	33.80	
	Posterior	Lateral	2.47	0.20	0.99	859.42	55.81	0.99
		Medial	2.55	0.24		900.81	39.81	
Middle	Anterior	Lateral	2.40	0.27	0.13	983.71	36.61	0.44
		Medial	2.44	0.23		978.55	6.17	
	Posterior	Lateral	2.77	0.44	0.44	894.67	15.25	0.13
		Medial	2.56	0.19		956.11	25.00	
Distal	Anterior	Lateral	2.11	0.17	0.063	899.55	18.86	0.19
		Medial	2.38	0.33		896.28	18.43	
	Posterior	Lateral	2.49	0.33	0.063	838.31	36.80	0.063
		Medial	2.21	0.32		922.16	10.23	

Table S1: Thickness and density of samples from each anatomical subsection (n=5/subsection). P-value results based on comparison of lateral vs medial samples within each anatomical quadrant. MAD = median absolute deviation.

Diaphysis	Quadrant	Test mode	Modulus (GPa)			Strength (MPa)			Plastic Deformation (mm)		
			Median	MAD	p-value	Median	MAD	p-value	Median	MAD	p-value
Proximal	Anterior	xSMS	5.08	0.92	0.81	151.34	6.33	0.31	0.14	4.5E-4	0.13
		SMS	4.72	0.49		165.35	19.80		0.22	0.03	
	Posterior	xSMS	3.07	0.65	0.81	101.60	3.15	0.81	0.53	0.12	0.063
		SMS	3.34	1.02		104.42	6.64		0.14	4.5E-4	
Middle	Anterior	xSMS	4.67	0.82	0.44	148.60	8.07	0.63	0.14	1.5E-4	0.81
		SMS	3.54	0.33		159.77	40.06		0.14	3.0E-4	
	Posterior	xSMS	2.28	0.22	0.19	92.57	11.06	0.31	0.40	0.06	0.063
		SMS	3.71	1.43		95.68	4.79		0.14	1.5E-4	
Distal	Anterior	xSMS	3.95	0.56	0.063	128.30	26.40	0.63	0.20	0.07	0.81
		SMS	3.24	0.66		124.55	4.23		0.30	0.24	
	Posterior	xSMS	2.69	0.71	0.31	98.55	4.59	0.31	0.42	0.09	0.063
		SMS	3.05	0.65		115.30	5.92		0.23	0.07	

Table S2: Modulus, bending strength, and plastic deformation of samples from each anatomical subsection (n=5/subsection). P-value results based on comparison of test mode (strain mode specific [SMS] vs non-strain mode specific [xSMS]) within each anatomical quadrant. Anterior: SMS = periosteal edge in tension, xSMS = periosteal edge in compression. Posterior: SMS = periosteal edge in compression, xSMS = periosteal edge in tension. MAD = median absolute deviation.